Geophysical Research Letters

RESEARCH LETTER
10.1029/2021GL092574

Observed Global Increases in Tropical Cyclone-Induced Ocean Cooling and Primary Production

Nguyen Dac Da[1,2], Gregory R. Foltz[2], and Karthik Balaguru[3]

[1]Cooperative Institute for Marine and Atmospheric Studies (CIMAS), Rosenstiel School of Marine and Atmospheric Science, University of Miami, Miami, FL, USA, [2]Atlantic Oceanographic and Meteorological Laboratory (AOML), National Oceanic & Atmospheric Administration, Miami, FL, USA, [3]Marine and Coastal Research Laboratory, Pacific Northwest National Laboratory (PNNL), Seattle, WA, USA

Key Points:

- Global tropical cyclone induced surface cooling and primary production has been increasing over the past 35 years
- The increasing trends of surface cooling and primary production are mainly attributed to increasing tropical cyclone intensity
- The decline in primary production induced by global warming has been partially negated by tropical cyclones in oligotrophic waters

Supporting Information:

Supporting Information may be found in the online version of this article.

Correspondence to:

N. D. Da,
nguyendacda@gmail.com

Citation:

Da, N. D., Foltz, G. R., & Balaguru, K. (2021). Observed global increases in tropical cyclone-induced ocean cooling and primary production. *Geophysical Research Letters*, *48*, e2021GL092574. https://doi.org/10.1029/2021GL092574

Received 21 JAN 2021
Accepted 27 MAR 2021

Abstract Tropical cyclones provide an important source of ocean mixing, bringing cold, nutrient-rich water to the surface and triggering phytoplankton blooms. Here, we show significant increases in global tropical cyclone-induced sea surface temperature cooling and surface chlorophyll-a concentration of 0.05°C and 3.7×10^{-3} mg m^{-3} per decade over the past 20–35 years. The trends have been driven primarily by an increase in the intensity of strong tropical cyclones. The increase in chlorophyll-a concentration has been, on average, 1.6% per decade in oligotrophic areas during the tropical cyclone season, in contrast to a decrease of 0.1% per decade during the other months. This tropical cyclone-induced increase has partially mitigated the overall decline in primary production under climate change.

Plain Language Summary Tropical cyclones (TCs) associated with strong wind can produce mixing in the upper ocean, bringing cold and nutrient-rich water in the subsurface to the surface and trigger photosynthesis. Therefore, they often leave trails on the surface of cold water and high Chlorophyll-a concentration, which can be observed from satellites. It is unknown how these interactions between TCs and the upper ocean change under global warming. In this study, based on satellite observations of sea surface temperature and Chlorophyll-a concentration over the past 20–35 years, we discover that ocean surface cooling and Chlorophyll-a concentration associated with TC activities have been increasing steadily. These changes are mainly attributed to the increasing intensity of strong (cat. 1–5) TCs. The increasing trend in primary production associated with TC activities can partially mitigate the declining trend of ocean productivity under global warming.

1. Introduction

The ocean absorbs more than 90% of the excess heat from anthropogenic forcing and has warmed steadily since the 1990s (Cheng et al., 2017), especially in the upper 200 m (Cheng et al., 2017; Li et al., 2020). Enhanced warming near the surface generates stronger stratification (Li et al., 2020), limiting the supply of nutrients to the euphotic layer (Boyce et al., 2010; Polovina et al., 2008). As a result, global ocean primary productivity, which accounts for half of the planet's net primary production (Field, 1998), is declining (Boyce et al., 2010; Gregg & Rousseaux, 2019), and the ocean's deserts are expanding (Polovina et al., 2008).

Anthropogenic warming has also driven changes in TC activity (Mei et al., 2015), including an increase in the frequency and intensity of the strongest TCs (Elsner et al., 2008; Mei et al., 2015; Webster, 2005), and has arguably decreased translation speed (Kossin, 2018; Lanzante, 2019). TCs are a significant source of mixing for the upper ocean, bringing cold subsurface water to the surface and causing SST cooling that acts to decrease the storm's intensity (Vincent et al., 2012). The cold water is also richer in nutrients, which can trigger phytoplankton blooms (Lin et al., 2003) and significantly contribute to the total ocean primary production in some regions (Foltz et al., 2015; Lin et al., 2003; Menkes et al., 2016). Thus, changes in TC frequency, intensity, and translation speed, which are crucial factors for TC-induced mixing, can potentially change the upper ocean's biophysical response. However, global changes in the ocean's response to TCs remain largely unexplored.

In this study, based on observed multidecadal trends in TC-induced SST cooling (cold wakes) and near-surface chlorophyll-a concentration increase (Chla wakes), we show for the first time how the response of the global upper ocean to TCs has been changing. We then investigate whether the changes in wakes are due to

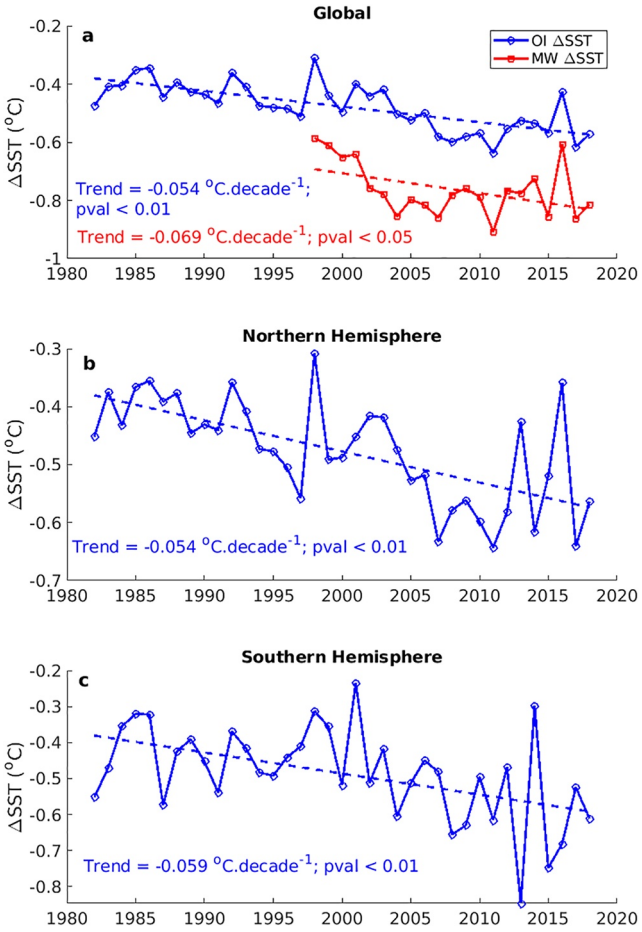

Figure 1. Interannual variations and trends of TC-induced cold wakes. (a) Global means from optimal interpolation (OI) and microwave (MW) SST datasets. The trends are 5×10^{-3} and 7×10^{-3}°C year^{-1} using OI and MW SST, respectively (b and c) Northern and Southern Hemisphere trends (5×10^{-3} and 6×10^{-3}°C year^{-1}, respectively) and interannual variability based on OI SST.

changes in TC activity, ocean stratification, or both. Finally, implications of the changes in the wakes for primary production are discussed.

2. Data and Methods

2.1. Data

Storm track data are obtained from the International Best Track Archive for Climate Stewardship (IBTrACS, Version 4, Knapp et al., 2018). This data set combines and unifies storm track data of different formats from different data centers in the world. In this study, we use the merged TC positions and maximum sustained wind speeds from the World Meteorological Organization (WMO) (lon, lat, and wmo_wind in the data file). IBTrACS data cover our study period (1982–2018) for all basins except the North Indian, for which wmo_wind is missing during the period before 1990.

For the computation of TC-induced SST cooling, we use the optimal interpolation (OI, version 2.0) daily SST data set provided by the National Centers for Environmental Information (NCEI, https://www.ncdc.noaa.gov/oisst), available since September 1981. OI SST combines in situ and infrared satellite observations, which can be impacted by clouds. We use OI SST because of its long period. For inter-validation, we use the microwave (MW, version 5.0) satellite SST data set produced by Remote Sensing Systems (www.remss.com). This daily SST data set is not impacted by clouds but is available only since 1998.

We obtained daily Chlorophyll-a concentration (Chla) from the Ocean Color Climate Change Initiative project (OCCI), version 3.1. This data set is distributed by European Space Agency and available online at http://www.esa-oceancolour-cci.org since September 1997. Chla retrievals are affected by clouds. However, the similarities between variability and trends of infrared and microwave SST in Figure 1 suggest that cloudiness is also unlikely to have a strong impact on the Chla variability and trends that we report.

Multiple ocean datasets are available and allow an ensemble view of ocean stratification. We use EN4, GODAS, ORAS4, and SODA. EN4 is an observational data set provided by the Met Office Hadley Center (https://www.metoffice.gov.uk/) and is available at monthly resolution from 1900 to present. GODAS is an ocean reanalysis data set produced by the National Centers for Environmental Prediction (NCEP, https://www.cpc.ncep.noaa.gov/). We use the monthly product, which is available from 1979 to present. ORAS4 is an ocean reanalysis data set produced by the European Center for Medium-Range Weather Forecasts (ECMWF) and distributed by the Integrated Climate Data Center (ICDC, https://icdc.cen.uni-hamburg.de/). The data set is available at monthly resolution and covers the period 1958–2017. SODA is an ocean reanalysis produced by Carton et al. (2018) and available at http://www.soda.umd.edu/. We use SODA version 3.3.2 at monthly resolution. This product covers the period 1980–2017.

Our analysis period for TC-induced SST cooling extends from 1982 (the first fully observed year of OI SST) to 2018, the most recent year of global storm track data in the IBTrACS data set. The TC-induced Chla analysis covers 1998 to 2018, when Chla and TC track data are available.

2.2. Trend Computation

Trends of TC-induced wakes and the factors that cause them are computed based on their annual mean time series.

2.2.1. Annual Index

In this study, we focus on long-term changes in the fast (1–3 days) upper-ocean response to TC forcing. At each TC's time-location, TC-induced SST cooling was computed as the difference in SST between the post-TC (1–3 days after) and pre-TC (2–4 days before) periods averaged over a 4° × 4° region centered at each TC's location. The same method was used to calculate TC-induced changes in Chla. The averaging periods were chosen to capture the strongest TC-induced surface signals (Balaguru, Leung, et al., 2020). The 4° length scale is equivalent to the mean diameter of 12 m s^{-1} sustained wind speed computed from more than 2,000 TCs observed by satellite scatterometer (Chavas & Emanuel, 2010) and is representative of the SST response to TCs (Balaguru, Leung, et al., 2020). The sensitivity of the choices of bin size and averaging period to the significance of TC-induced SST cooling and Chla trends have also been tested (see Tables S1–S4). For each calendar year, the SST cooling is then averaged over all TC locations for which the maximum sustained wind speed is higher than 33 m s^{-1} (64 kt) in order to form an annual time series. For the Chla index, we limit to TC locations in offshore regions defined as follows: Northwest Pacific (128E–151E; 16N–30N), Northeast Pacific (130W–110W; 10N–22N), North Atlantic (70W–35W; 25N–38N), South Indian (52E–113E; 10S–20S), and South Pacific (155E–160W; 10S–30S). The combined region takes into account data in all of these offshore regions. The locations and sizes of the regions are illustrated in Figure S1 in the supplementary document. Limiting to open-ocean regions reduces contamination from rivers and other coastal processes, such as upwelling. Chla data in coastal areas are also known to have higher uncertainties (Moore et al., 2009).

Annual mean temperature profiles are computed over TC-active tropical areas (Figure S2). Annual temperature stratification (Grad-T) is then computed from the annual mean temperature profiles as the gradient of temperature in the upper 100 m of the ocean (Da et al., 2020). This depth was found to be relevant for TC studies (Balaguru, Foltz, et al., 2020; Da et al., 2020). To calculate Grad-T, we fit all data from each profile to a simple linear regression model, $y = ax + b$, where y is the temperature of the profile, x is the corresponding depth, b is a constant, and a represents the temperature gradient (Grad-T) in the upper 100 m.

2.3. Trend Significance

The significance levels of trends are assessed with both the p-value and 95% confidence intervals. P-values for trends are obtained from a Student's t-test (function regstats in Matlab 2019), and their confidence intervals are computed using a bootstrapping method. For a given year, we randomly sample the data with replacement 1,000 times to obtain 1,000 different estimations of the annual index. This process is repeated for the whole period to create 1,000 different annual time series. The trends of the time series are then derived by fitting a linear model $y = ax + b$ to the data, where y is the linear prediction of the annual index, x is the year, b is a constant, and a represents the trend values. The confidence interval for a trend is calculated as the 2.5 to 97.5 percentile interval of these 1,000 values of a.

2.4. Attribution of the Trends

Both TC characteristics and ocean stratification can have impacts on TC induced cold wake trends and Chla trends. With the assumption that the effects of the factors driving cold wake and Chla wake trends are similar, we assess the relative roles of TC characteristics and ocean stratification on cold wake trends only.

2.4.1. 1D-Theoretical Model of Cold Wake

To compare the relative impacts of ocean stratification and TC characteristics on cold wake trends, we adopt the method described in Balaguru et al. (2015). The method provides a theoretical estimate of oceanic mixing induced by a TC with given intensity, translation speed, and subsurface ocean temperature and salinity that vary only with depth (i.e., stratification can be characterized using a single temperature-salinity profile). This mixing length represents the new mixed layer after mixing induced by the TC. Temperature is considered to be constant within the new mixed layer. The mean temperature of the original profile over the new mixing length represents the post-TC SST, which can then be used to derive SST cooling driven by different factors (e.g., TC intensity, translation speed, ocean stratification).

We limit our analysis to tropical areas (within 30N–30S, Figure S2), where stratification is strongest and TCs are the most active. We compute annual mean indices for TC intensity and translation speed using the method described above (Section 2.2.1). We then obtain mean temperature profiles for each year using the GODAS data set, from which TC-season mean temperature stratification is computed. The TC-induced mixed layer deepening for a given pair of temperature and salinity profiles is computed as follows (Balaguru et al., 2015):

$$\Delta MLD = \left(\frac{2\rho_0 u*^3 t}{\kappa g \alpha} \right)^{\frac{1}{3}}$$

where ρ_0 is the sea water density, u_* is friction velocity which is proportional to TC intensity, t is the time period of mixing and is inversely proportional to TC translation speed, κ is the von Kármán constant, g is the acceleration due to gravity, and α is density stratification beneath the mixed layer of the seasonal mean profile. To isolate the effects of TC intensity ($u*$), translation speed (t), and ocean stratification (α) variations on ΔMLD, we let one of the three factors vary while the other two are fixed at their mean values. In this study, we consider TCs with maximum sustained wind speed >33 m s^{-1} (category 1–5 in the Saffir-Simpson wind scale). This gives a mean TC wind speed of 44 m s^{-1} and mean translation speed of 4.9 m s^{-1}. The mean density stratification at the base of the mixed layer (α) averaged in the tropics is about 0.024 kg m^{-4}. Post-TC SST is then obtained by averaging the initial temperature profile vertically over the total mixing length, which is $MLD + \Delta MLD$, where MLD is the pre-TC mixed layer depth defined as the depth where the density has increased 0.125 kg.m^{-3} with respect to its value at the depth of 10 m. SST-cooling is the difference between post- and pre-TC SST. When stratification is fixed at its mean value, the record-length seasonal-mean initial mixed layer depth and temperature profile are also used.

2.4.2. Spatial Relationships Between Cold Wake and TC Parameters

There is not enough data to compute maps of trends in cold wakes and TC intensity to show their spatial relationships. We therefore illustrate their spatial relationships by computing their decadal differences, defined for each quantity in every 5° × 5° bin as the mean of the annual index over the last decade (2009–2018) minus the mean over the first decade (1982–1991). Decadal maps of ocean stratification are computed over TC seasons (June–November and January–June for the Northern and Southern hemisphere, respectively) and are resampled to the same resolution of the other indexes. The resulting maps are shown in Figure S3 and their spatial correlations are shown in Table S5.

2.5. Implications for Primary Production

In the context of declining ocean productivity in oligotrophic areas (see Section 1), are changes in TC-induced Chla wakes strong enough to alter the general declining trend? To answer this question, we compute seasonal mean Chla concentration over TC seasons and non-TC seasons. TC seasons in the Northern and Southern Hemispheres are from June to November and from January to June, respectively. Non-TC seasons are the other months of the year. Daily Chla concentrations within the offshore regions (Figure S1) are averaged over the respective seasons and the corresponding areas to obtain the seasonal Chla indices of the regions. The global offshore seasonal Chla index is then computed as the area-weighted average of all offshore regions.

3. Results

3.1. Cold Wake Trend

We find consistent increases in cold wakes (i.e., more TC-induced cooling) of 0.05°C–0.06°C per decade in the Northern and Southern Hemispheres and at the global scale since 1982 (Figure 1). The significance of the trends is insensitive to different time periods and averaging areas. The corresponding cold wake trends for individual basins are summarized in Table 1. All show significant increases in cooling ranging from 0.04°C to 0.08°C per decade, weakest in the North Atlantic and strongest in the North Indian. The highest negative trend in the North Indian Ocean may result partly from the fact that it is calculated over a more

Table 1
Trends and 95% Confidence Intervals (Numbers in Brackets) of TC-Induced SST Cooling and Primary Production in Different basins

		North Atlantic	Northwest Pacific	Northeast Pacific	North Indian	South Indian	South Pacific	Global
Whole basin	SST-cooling trend (10^{-} 2° C decade^{-1})	**−4.3** [−5.5, −3.2]	**−4.4** [−5.2, −3.7]	**−5.3** [−6.3, −4.5]	**−8.0** [−11.1 −4.8]	**−5.5** [−6.7, −4.4]	**−4.9** [−5.9, −3.9]	**−5.4** [−5.8, −5.0]
Offshore Area	Chla Trend (10^{-3} mg m^{-3} decade^{-1})	**2.1** [0.6, 3.3]	**4.1** [2.7, 5.5]	**4.9** [3.2, 6.7]	-	**7.0** [5.1, 9.1]	**6.5** [4.1, 8.8]	**3.7** [2.9, 4.4]
	Detrended correlation (SST, Chla)	**−0.49** [−0.68, −0.29]	**−0.45** [−0.59, -0.32]	**−0.40** [−0.59, −0.21]	-	**−0.40** [−0.52, −0.28]	**−0.47** [−0.63, −0.31]	**−0.32** [−0.45, −0.19]

All trends are significant at the 95% level. In the North Indian Ocean, the size of the offshore region with TC activity is too small to be considered (see Figure S1).

recent and shorter period (1990–2018) due to limitations in the availability of TC track data (see Data and Methods for more details).

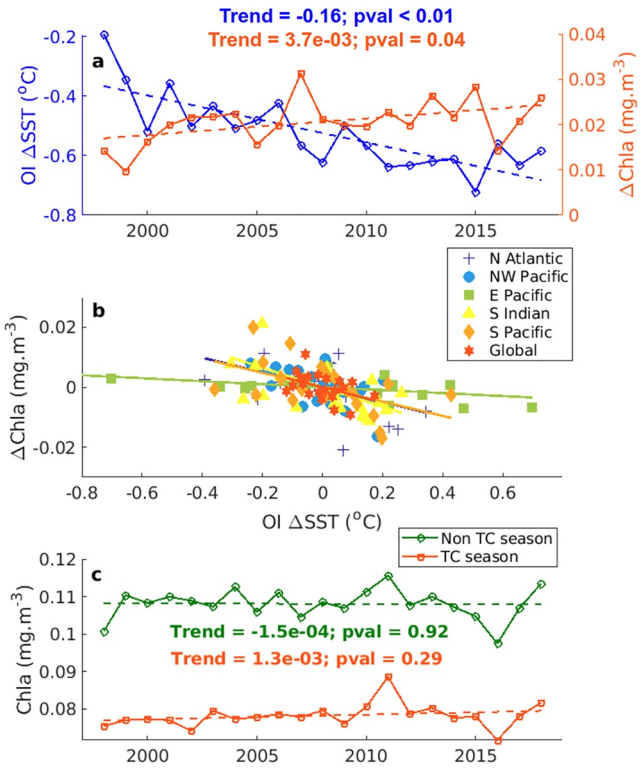

Figure 2. Trends and variability of Chla and its relationship with SST cooling. (a) Annual means and trends of TC-induced Chla (orange, mg m^{-3} decade^{-1}) and corresponding SST cooling (°C decade^{-1}) over the global oligotrophic regions shown in Figure S1. (b) Detrended relationships between Chla and SST cooling in different basins. The respective correlations are shown in Table 1. (c) is similar to (a) but for seasonal mean Chla concentration averaged over the TC season and the non-TC season. TC seasons are June–November and January–June in the Northern and Southern Hemispheres, respectively. Non-TC seasons are the other months of the year.

The SST record going back to 1982 combines in situ and infrared satellite data (hereafter, OI SST) and is therefore sensitive to clouds, especially in the presence of TCs. To verify the global variability and trends of cold wakes, we use daily microwave (MW) satellite SST, which is available since 1998 and is less affected by clouds. Compared to OI SST, the cold wakes computed from MW SST display a consistent and stronger global trend of 0.07°C per decade (Figure 1a). The OI and MW SST interannual variations also agree well over their common period, with a detrended correlation of 0.60 that is significant at the 99% level. Therefore, the increasing trend of global cold wakes is significant and robust.

3.2. Chla Wake Trend

Next we look at TC-induced changes in primary production based on satellite Chlorophyll-a concentration (Chla hereafter for short). Figure 2a shows that TC-induced Chla has a significant positive global trend of 3.7×10^{-3} mg m^{-3} per decade for the period 1998–2018, consistent with the increasing trend of cold wakes. The significant global Chla trend results from significant trends at the 95% level from all of the basins (Table 1). Chla trends in individual basins range from 2.1 to 7.0×10^{-3} mg m^{-3} per decade and are stronger in the Southern Hemisphere than the Northern Hemisphere. Chla trends are slightly more sensitive to time and area averaging than cold wake trends, partly due to the shorter time record. TC-induced Chla varies out of phase with TC-induced SST cooling in all basins and globally: stronger cooling is associated with enhanced Chla (Figure 2, Table 1). All regions have correlations that are larger than 0.32, are significant at more than 95%, and are robust to different time- and area-averaging. Together, the trends in TC-induced cold wakes and Chla are compelling evidence for the increasing efficiency with which TCs are pumping cold, nutrient-rich water to the euphotic zone and consequently enhancing oceanic primary production.

3.3. Mechanisms of the Trends

The opposing trends in TC-induced SST and Chla wakes, and their strong negative correlation on interannual timescales, suggest there may be a

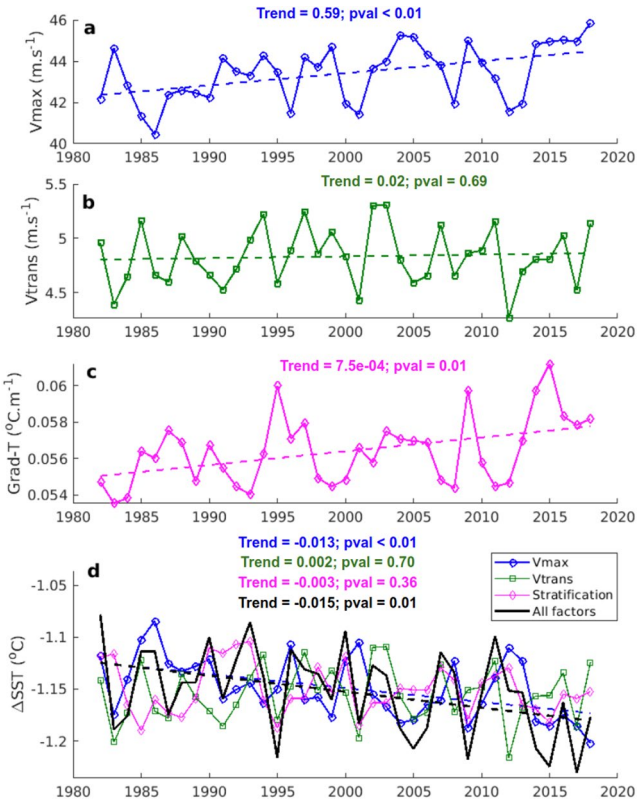

Figure 3. Variability and trends of factors that drive cold wake and Chla trends. Annual mean (a) intensity and (b) translation speed for storms with sustained wind speed greater than 33 m s^{-1} (equivalent to category 1–5 on the Saffir-Simpson wind scale). (c) Annual mean temperature stratification in the upper 100 m averaged over TC seasons: June–November and January–June in the Northern and Southern Hemisphere, respectively. Both TC characteristics and ocean stratification are computed over TC-active tropical areas: 10°N–30°N in the Northern Hemisphere and 10°S–30°S, 30°E–160°W in the Southern Hemisphere (see Figure S2). (d) Impacts of individual factors and their sum on cold wake variability and trends (numbers shown in a–d are per decade), computed from a theoretical approach (see Data and Methods).

common cause: Either from changes in TC characteristics (intensity and translation speed) or from changes in ocean stratification, or both. To address this, we analyze the factors within the tropics and during the TC seasons: June to November in the Northern Hemisphere and January to June in the Southern Hemisphere (Figure S2).

For TCs with maximum sustained wind speed >33 m s^{-1} (category 1–5 in the Saffir-Simpson wind scale), translation speed does not have a significant trend and therefore cannot be the cause of the SST and Chla wake trends (Figures 3b and 3d). In contrast, both TC intensity and temperature stratification have highly significant trends (at more than 99% level) of 0.59 m s^{-1} and 7.5×10^{-4} °C m^{-1} per decade, respectively (Figures 3a and 3c). The increase in TC wind forcing has increased the TC-induced ocean mixing length by 0.43 m per decade, and the enhanced stratification has decreased the mixing length by 0.27 m per decade (Data and Methods and Figure S3), both significant at the 99% level. The increase in TC intensity has driven a cold wake trend of 0.013°C per decade (significant at 99%), consistent with the increase in mixing length (Figure 3d). However, the cold wake trend caused by the ocean stratification trend is much weaker (0.003°C per decade) and insignificant. This is because enhanced temperature stratification has opposing effects on SST cooling, acting to reduce TC-induced mixing and cooling due to increased stability while also tending to increase cooling because colder water is closer to the surface. The positive trend in cold wakes of 0.003°C per decade associated with enhanced stratification implies that the latter effect is stronger, but not strong enough to result in a significant cold wake trend. Therefore, the global cold wake trend of 0.015°C per decade is mainly due to strengthening of ocean turbulent mixing caused by an increase in TC intensity. Note that in our analysis, we did not consider the role of Ekman pumping in the observed SST cooling and Chla, which may be an important factor for slow-moving TCs (Price, 1981). However, since there is no significant trend in TC translation speed, we believe that TC-induced mixing is likely the main driver of the upward trends in SST cooling and primary production. TC-induced rainfall may also have small but significant impacts on SST and Chla wake magnitudes (Jourdain et al., 2013; Lin and Oey, 2016). Separating the integrated impacts of rainfall and ocean mixing on TC-induced SST and Chla wakes is complex and will require further work. Coastal upwelling can also affect TC-induced SST and Chla wakes in limited areas (e.g., Scrosati 2020) and deserves additional study.

When we extend the analysis to include all TCs with maximum sustained wind speed greater than 17 m s^{-1} (i.e., tropical storms in the Saffir-Simpson wind scale, Figure S4), the trend in translation speed remains similar (0.01 m s^{-1} per decade) and insignificant, and the trend in annual mean TC intensity becomes much weaker and insignificant, decreasing from 0.59 to 0.11 m s^{-1} per decade. Therefore, the observed SST and Chla trends have been caused primarily by positive trends in the intensities of category 1–5 TCs.

Maps of decadal differences (2009–2018 vs. 1982–1991) between TC intensity and cold wake (see Data and Methods and Figure S5) provide further evidence that the increase in intensity of category 1–5 TCs is the main driver of the trends in TC-induced SST and Chla wakes. The spatial correlation between decadal differences in TC intensity and cold wake is −0.49, which is significant at the 99% level. Temperature stratification trends from different datasets, however, show mixed and highly variable spatial correlations with cold wake trends (from −0.30 to +0.27), despite consistent positive trends in stratification averaged across the global tropics (Figures S6, Table S1).

4. Discussion

The significant upward trends of global TC-induced SST cooling and Chla reported here are evidence of enhanced TC-induced mixing caused by the strengthening of high-intensity TCs (categories 1–5). The positive trend of TC-induced primary production in oligotrophic areas of 3.7×10^{-3} mg m^{-3} per decade is about 4.0% of the annual mean Chla of 0.093 mg m^{-3} in those regions (Figures 2a and 2c). This significant enhancement of along-track TC-induced Chla is strong enough to induce a positive trend in Chla (1.6% per decade) when averaged over all oligotrophic areas for the entire TC season (Figure 2c). In contrast, the Chla trend averaged in the same regions for non-TC seasons is −0.1% per decade. This integrated effect of TCs on seasonal Chla is present in the offshore regions of three out of the five TC basins including Northwest Pacific, South Indian, and South Pacific (Figure S8), and is highly significant over the South Pacific. The increase of 1.6% per decade, averaged over all oligotrophic regions, is similar but opposite in sign to the declining rate of global primary production of −2.1% per decade suggested by Gregg and Rousseaux (2019) over the similar period of 1998–2015. The increasing trend of Chla from TCs illustrates the potential for TCs to partially mitigate some of the negative consequences of desertification in offshore oligotrophic areas and highlights the complexity of global warming's impact on the ocean's biosphere.

Data Availability Statement

All data used in this study are available publicly from the following websites: Storm track data: https://www.ncdc.noaa.gov/ibtracs/; OI SST data: https://www.ncdc.noaa.gov/oisst; MW SST data: www.remss.com; Chla data: http://www.esa-oceancolour-cci.org; EN4 data: https://www.metoffice.gov.uk/; GODAS data: https://www.cpc.ncep.noaa.gov/; ORAS4 data: https://icdc.cen.uni-hamburg.de/; SODA data: http://www.soda.umd.edu/

Acknowledgments
NDD and GF were supported by the Climate Observations and Monitoring Division of NOAA's Climate Program Office and base funds to NOAA/AOML's Physical Oceanography Division. KB acknowledges support from NOAA's Climate Program Office, Climate Monitoring Program (Award Number: NA17OAR4310155). KB is also supported by the Office of Science (BER) of the U.S. Department of Energy as part of the Regional and Global Modeling and Analysis (RGMA) Program. The Pacific Northwest National Laboratory is operated for DOE by Battelle Memorial Institute under contract DE-AC05-76RL01830.

References

Balaguru, K., Foltz, G. R., Leung, L. R., Asaro, E. D., Emanuel, K. A., Liu, H., & Zedler, S. E. (2015). Dynamic Potential Intensity: An improved representation of the ocean's impact on tropical cyclones. *Geophysical Research Letters*, *42*(16), 6739–6746. https://doi.org/10.1002/2015gl064822

Balaguru, K., Foltz, G. R., Leung, L. R., Kaplan, J., Xu, W., Reul, N., & Chapron, B. (2020). Pronounced impact of salinity on rapidly intensifying tropical cyclones. *Bulletin of the American Meteorological Society*, *101*(9), E1497–E1511. https://doi.org/10.1175/bams-d-19-0303.1

Balaguru, K., Leung, L. R., Van Roekel, L. P. V., Golaz, J.-C., Ullrich, P. A., Caldwell, P. M., et al. (2020). Characterizing tropical cyclones in the energy exascale earth system model Version 1. *Journal of Advances in Modeling Earth Systems*, *12*(8), e2019MS002024. https://doi.org/10.1029/2019ms002024

Boyce, D. G., Lewis, M. R., & Worm, B. (2010). Global phytoplankton decline over the past century. *Nature*, *466*(7306), 591–596. https://doi.org/10.1038/nature09268

Carton, J. A., Chepurin, G. A., & Chen, L. (2018). SODA3: A new ocean climate reanalysis. *Journal of Climate*, *31*, 6967–6983. https://doi.org/10.1175/jcli-d-18-0149.1

Chavas, D. R., & Emanuel, K. A. (2010). A QuikSCAT climatology of tropical cyclone size. *Geophysical Research Letters*, *37*(18). https://doi.org/10.1029/2010gl044558

Cheng, L., Trenberth, K. E., Fasullo, J., Boyer, T., Abraham, J., & Zhu, J. (2017). Improved estimates of ocean heat content from 1960 to 2015. *Science Advances*, *3*(3), e1601545. https://doi.org/10.1126/sciadv.1601545

Da, N. D., Foltz, G. R., & Balaguru, K. (2020). A satellite-derived upper-ocean stratification data set for the tropical north Atlantic with potential applications for hurricane intensity prediction. *Journal of Geophysical Research: Oceans*, *125*(10), e2019JC015980. https://doi.org/10.1029/2019jc015980

Elsner, J. B., Kossin, J. P., & Jagger, T. H. (2008). The increasing intensity of the strongest tropical cyclones. *Nature*, *455*(7209), 92–95. https://doi.org/10.1038/nature07234

Field, C. B. (1998). Primary production of the biosphere: Integrating terrestrial and oceanic components. *Science*, *281*(5374), 237–240. https://doi.org/10.1126/science.281.5374.237

Foltz, G. R., Balaguru, K., & Leung, L. R. (2015). A reassessment of the integrated impact of tropical cyclones on surface chlorophyll in the western subtropical North Atlantic. *Geophysical Research Letters*, *42*(4), 1158–1164. https://doi.org/10.1002/2015gl063222

Gregg, W. W., & Rousseaux, C. S. (2019). Global ocean primary production trends in the modern ocean color satellite record (1998–2015). *Environmental Research Letters*, *14*(12), 124011. https://doi.org/10.1088/1748-9326/ab4667

Jourdain, N. C., Lengaigne, M., Vialard, J., Madec, G., Menkes, C. E., Vincent, E. M., et al. (2013). Observation-based estimates of surface cooling inhibition by heavy rainfall under tropical cyclones. *Journal of Physical Oceanography*, *43*(1), 205–221. https://doi.org/10.1175/jpo-d-12-085.1

Knapp, K. R., Diamond, H. J., Kossin, J. P., Kruk, M. C., & Schreck, C. J. (2018). International Best Track Archive for Climate Stewardship (IBTrACS) Project, Version 4. NOAA National Centers for Environmental Information.[05/27/2020]. https://doi.org/10.25921/82ty-9e16

Kossin, J. P. (2018). A global slowdown of tropical-cyclone translation speed. *Nature*, *558*(7708), 104–107. https://doi.org/10.1038/s41586-018-0158-3

Lanzante, J. R. (2019). Uncertainties in tropical-cyclone translation speed. *Nature*, *570*(7759), E6–E15. https://doi.org/10.1038/s41586-019-1223-2

Li, G., Cheng, L., Zhu, J., Trenberth, K. E., Mann, M. E., & Abraham, J. P. (2020). Increasing ocean stratification over the past half-century. *Nature Climate Change*, *10*, 1116–1123.

Lin, I., Liu, W. T., Wu, C.-C., Wong, G. T. F., Hu, C., Chen, Z., et al. (2003). New evidence for enhanced ocean primary production triggered by tropical cyclone. *Geophysical Research Letters*, *30*(13), 1718. https://doi.org/10.1029/2003gl017141

Lin, Y.-C., & Oey, L.-Y. (2016). Rainfall-enhanced blooming in typhoon wakes. *Scientific Reports*, *6*, 31310. https://doi.org/10.1038/srep31310

Mei, W., Xie, S.-P., Primeau, F., McWilliams, J. C., & Pasquero, C. (2015). Northwestern Pacific typhoon intensity controlled by changes in ocean temperatures. *Science Advances*, *1*(4), e1500014. https://doi.org/10.1126/sciadv.1500014

Menkes, C. E., Lengaigne, M., Lévy, M., Ethé, C., Bopp, L., Aumont, O., et al. (2016). Global impact of tropical cyclones on primary production. *Global Biogeochemical Cycles*, *30*(5), 767–786. https://doi.org/10.1002/2015gb005214

Moore, T. S., Campbell, J. W., & Dowell, M. D. (2009). A class-based approach to characterizing and mapping the uncertainty of the MODIS ocean chlorophyll product. *Remote Sensing of Environment*, *113*(11), 2424–2430. https://doi.org/10.1016/j.rse.2009.07.016

Polovina, J. J., Howell, E. A., & Abecassis, M. (2008). Ocean's least productive waters are expanding. *Geophysical Research Letters*, *35*(3). https://doi.org/10.1029/2007gl031745

Price, J. F. (1981). Upper ocean response to a Hurricane. *Journal of Physical Oceanography*, *11*(2), 153–175. https://doi.org/10.1575/1912/10271

Scrosati, R. A. (2020). Cyclone-driven coastal upwelling and cooling depend on location relative to the cyclone's path: Evidence from Dorian's arrival to Atlantic Canada. *Frontiers in Marine Science*, *7*, 651. https://doi.org/10.3389/fmars.2020.00651

Vincent, E. M., Lengaigne, M., Vialard, J., Madec, G., Jourdain, N. C., & Masson, S. (2012). Assessing the oceanic control on the amplitude of sea surface cooling induced by tropical cyclones. *Journal of Geophysical Research*, *117*, C05023. https://doi.org/10.1029/2011jc007705

Webster, P. J. (2005). Changes in tropical cyclone number, duration, and intensity in a warming environment. *Science*, *309*(5742), 1844–1846. https://doi.org/10.1126/science.1116448